measured but is at the level of 0.2–0.6 c$\bar{\text{c}}$ pairs per Pb–Pb interaction at 158$A$ GeV. Thus, only one in about 2000 c$\bar{\text{c}}$ pairs produced emerges as a bound J/$\Psi$(c$\bar{\text{c}}$) state. The uncertainty in this estimate is at least a factor of two and depends on the centrality of the interaction. It is hoped that further experimental information will become available soon, allowing us to understand this ratio more precisely.

The excited state $\Psi'$ has a yield five times smaller. There has not yet been a measurement of production of the other onium states in nuclear collisions.

In the LHC energy range, one can expect that the bound state of b-quarks, the upsilonium $\Upsilon(\bar{\text{b}}\text{b})$, will assume a similar role to that which is today being played, at SPS and RHIC energies, by J/$\Psi$.

The other heavy-quark bound state that is of interest is the B$_{\text{c}}$($\bar{\text{b}}$c). This quarkonium state is so rarely produced that it was not discovered until very recently [9, 10]. However, it has been studied extensively theoretically, and the currently reported mass, $M = 6.4 \pm 0.39 \pm 0.13$ GeV, is in good agreement with the theoretical quark-potential model expectations. The life span, $\tau \simeq 0.5$ ps, $c\tau \simeq 150\,\mu$m, implies that the current silicon pixel detector technology allows one to distinguish the production vertex from the B$_{\text{c}}$($\bar{\text{b}}$c) decay vertex.

The conventional mechanism for production of B$_{\text{c}}$($\bar{\text{b}}$c) requires the formation of two pairs of heavy quarks in one elementary interaction, followed by the formation of a bound state. The probability of these three unlikely events occurring in one interaction is not large and hence neither is the relative predicted yield, $(\text{B}_{\text{c}} + \text{B}_{\text{c}}^*)/(\text{b}, \bar{\text{b}}) \simeq (3\text{–}10) \times 10^{-5}$ at $\sqrt{s_{\text{NN}}} = 200$ GeV [169]. This small value implies that 'directly' produced B$_{\text{c}}$ (both in $J = 0$ and $J = 1$ channels B$_{\text{c}}^*$ and $\bar{\text{B}}_{\text{c}}^*$) cannot be observed at the RHIC. On the other hand, an enhancement in production of this state is expected in the QGP-mediated recombination [239], which could lead to a measurable rate of production in nuclear interactions. Since the quark-recombination mechanism of production requires mobility of heavy color-charged quarks, observation of this new mechanism for the formation of this exotic meson would constitute another good signature of the deconfined QGP phase.

# 3 The vacuum as a physical medium

## 3.1 Confining vacuum in strong interactions

Theoretical interest in the study of relativistic heavy-ion collisions originates, in part, from the belief that we will be able to explore the vacuum structure of strong interactions and, in particular, the phenomenon of quark confinement. The picture of confinement can be summarized as

follows:

1. all strongly interacting particles are made of quarks and gluons;
2. quarks q and gluons g are *color* charged [123], but all asymptotic observable physical states they can form are color neutral;
3. therefore, the *true* vacuum state $|V\rangle$ abhors color;
4. there is an excited state $|P\rangle$, referred to as *perturbative vacuum*, in which colored particles can exist as individual entities and therefore move freely;
5. $|P\rangle$ differs essentially from $|V\rangle$, the true vacuum, and in particular, it differs by a considerable amount of energy density in the regions of space–time in which the $|V\rangle$ structure is dissolved into $|P\rangle$.

In the 'true vacuum' (in which we live), color-charged quarks and gluons are 'confined'. However, under extreme conditions of density and temperature, we should reach the crossover to the color-conductive phase of the vacuum. In such a space–time domain, nearly free propagation of colored quarks and gluons is thought possible. This picture of hadronic interactions is consistent and indeed justifies the perturbative approach to quantum-chromodynamics (QCD) interactions. It is the foundation that allows us to describe hadrons as bags, i.e., confined bound states of quarks, see section 13.2. We also use these simple, but essential, features in the discussion of the physical properties of the QGP state in section 4.6. The melted color-conductive state $|P\rangle$ is a locally excited space–time domain in which quarks and gluons can move around. This state has properties that we would like intuitively to associate with a normal physical state, since it is simple, structureless. We must keep in mind that the situation is, however, inverted relative to our expectations. Since quarks and gluons are not observed individually, they cannot propagate in the true vacuum state, thus the true physical 'ground' state $|V\rangle$ must be complex and structured, and it is the excited state that is simple and structureless.

Vacuum structure keeps the colored particles bound and confined. Quark confinement has not been explained to be a direct result of quark–quark interaction, generated by the color charge and exchange of gluons. Rather, this force determines within a domain of perturbative vacuum $|P\rangle$ the structural detail: for the ground state the structure of the hadronic spectrum; at sufficiently high excitation, the properties of the color plasma of hot quarks and gluons. To be able to move color charges within a region of space, one needs to 'melt' the confining structure. For a first-order phase transition, the two phases have a difference in energy density, the latent heat $\mathcal{B}$, per unit of volume,

$$\boxed{\mathcal{B} \equiv \epsilon^{\mathrm{QGP}}(T_{\mathrm{cr}}, V_{\mathrm{cr}}; b) - \epsilon^{\mathrm{HG}}(T_{\mathrm{cr}}, V_{\mathrm{cr}}; b) \approx 0.5 \text{ GeV fm}^{-3}.} \qquad (3.1)$$

We would like to determine, by studying the QGP phase, the magnitude of $\mathcal{B}$. So far, only relativistic nuclear collisions can deliver (to a large region of space) the required energy and are the best and only tool we have today to study the process of melting of the QCD vacuum, see section 5.2. We will discuss the experimental methods further in chapter 5.

The vacuum properties of strong interactions can be explored only when the locally deconfined state, the QGP, is experimentally established. In our opinion, the study of the physical properties of the hadronic vacuum, in particular 'confined vacuum melting', is the fundamental challenge motivating the high-energy nuclear-collision experimental program. It is relevant to note that the key ideas and concepts underpinning the possibility of finding the vacuum 'melting' are robust against change and evolution of our knowledge: neither the questions about the existence of a true (discontinuous) phase transition between the hadronic vacuum states nor the possible quark substructures will greatly influence these considerations. All we want is to determine that the color-melted state contains particle-like quark–gluon excitations with established symmetries and interactions.

The most interesting property of the true QCD vacuum $|V\rangle$ is that it abhors the color charge of quarks and gluons. However, we are interested in determining and understanding its other physical properties. The appearance of a glue 'condensate' field, i.e., the vacuum expectation value of the 'square' of the gluon field, the so-called field-correlator in the true vacuum state [242, 243], is of particular relevance for the understanding of $|V\rangle$. With the glue fields defined as in section 13.4 we have

$$\frac{1}{2}F^2 \equiv \sum_a \frac{1}{2}F^a_{\mu\nu}F_a^{\mu\nu} = \sum_a [\vec{B}_a^2 - \vec{E}_a^2], \tag{3.2}$$

where we use Einstein's summation convention for repeated Greek indices.

The value of $F^2$ is obtained by studying QCD sum rules [197, 198, 242, 243], and is in agreement with the results obtained numerically using lattice-gauge-theory methods [100, 101]:

$$\Delta F^2 \equiv \langle V|\frac{\alpha_s}{\pi}F^2|V\rangle - \langle P|\frac{\alpha_s}{\pi}F^2|P\rangle \simeq (2.3 \pm 0.3) \times 10^{-2}\,\text{GeV}^4, \tag{3.3}$$

$$= [390 \pm 12\,\text{MeV}]^4.$$

Here, $\alpha_s = g_s^2/(4\pi)$ is the coupling constant for the strong interaction. Since in empty space the vacuum state is field-free, i.e., the vacuum expectation value of the gauge field vanishes, the appearance of a non-vanishing vacuum expectation value of the square of the gauge field in Eq. (3.3) is a quantum effect without a classical analog.

## 3.2 Ferromagnetic vacuum

We now describe a model and discuss other properties of the vacuum state that are related to the remarkable result Eq. (3.3). Because of the non-abelian nature of color charges, the quanta that mediate the color force, gluons, can themselves interact by means of exchanging gluons. Since gluons are massless, there is no energy gap that would stabilize their number. An attractive force between them will induce a major realignment in the perturbative wave function, i.e., $|P\rangle$, of the many-body gluon system.

Upon inserting Eq. (3.2) into Eq. (3.3), we see that the color $B$-field (magnetic) fluctuations dominate the color $E$-field (electrical) fluctuations:

$$\Delta \sum_a \vec{B}_a^2 = \Delta \sum_a \vec{E}_a^2 + 2[390 \pm 12\,\mathrm{MeV}]^4. \tag{3.4}$$

Here, $\Delta$ is defined as on the left-hand side of Eq. (3.3). The natural interpretation of this equation is that the true vacuum structure is predominantly magnetic. Indeed, an instability of the perturbative vacuum of QCD toward the formation of a ferromagnetic structure, was discovered early on in the development of QCD [56, 187, 236]. This effect has been shown to arise due to the attractive magnetic spin–spin interaction of gluons [35, 199, 200]. This spontaneous ferromagnetic instability parallels, in many important aspects, the instability in QED vacuum in the presence of constant electro-magnetic (EM) fields.

In QED, in the presence of a constant electrical field $E$, there is a nonvanishing probability of spontaneous particle-pair formation, with the probability per unit time and volume given by [240]

$$w = \frac{\alpha \vec{E}^2}{\pi^2} \sum_{n=1}^{\infty} \frac{1}{n^2} \exp\left(-n\frac{\pi m^2}{|e\vec{E}|}\right). \tag{3.5}$$

The electromagnetic fine-structure constant, $\alpha \simeq 1/137$, is relatively small, and the mass $m$ of the lepton (electron) produced is large compared with the laboratory fields available. Thus, in fact, this process has never been observed. The physical origin of the QED vacuum instability resides in the fact that, in a constant infinitely extending field, we can always find a potential difference between two distant points that exceeds the pair mass, and thus spontaneous pair production can ensue [219]. Schwinger's rate Eq. (3.5) is arising in such a description from the process of quantum tunneling through a barrier that the potential $V = \int d\vec{x}\vec{E}$ implies, and therefore it can be adapted with ease to the study of QCD [88, 132]. This mechanism is serving as the basis for particle production within the color string models, in which breaking of the color-electrical-flux tube

connecting rapidly separating quarks provides the mechanism for particle production [39].

In the case of QED, the particles produced are screening the field source, and the vacuum-state energy still has a local minimum around the perturbative vacuum-state configuration with vanishing EM fields. In this regard the situation is different in QCD, in which there is a ferromagnetic instability. To understand this QCD magnetic instability, recall that, in a constant magnetic field of magnitude $B$, a particle with spin projection $\sigma$ and orbital momentum $l = 1, 2, 3, \ldots$, with reference to the direction of $B$ has the Landau energy

$$E_{l\sigma}^2 = m^2 + k_\parallel^2 + 2g_{\mathrm{s}}B(l + \sigma + \tfrac{1}{2}), \qquad (3.6)$$

and the effective degeneracy is

$$g_B = \frac{V^{2/3}}{2\pi} g_{\mathrm{s}}B. \qquad (3.7)$$

For $\sigma = -\frac{1}{2}$ (leptons, quarks), the lowest energy level for $k_\parallel = l = 0$ is at $E_0^2 = m^2$, as is seen in Eq. (3.6). However, for spin-1 gluons, states with $\sigma = -1$ display an instability whereby $E_0^2$ becomes negative for $gB > m^2 = g_{\mathrm{s}}B_{\mathrm{cr}}$. For gluons with $m_{\mathrm{g}} = 0$, this occurs for an arbitrarily small value of $B$. Therefore, the spectrum of Landau states begins at a minimum momentum, $k_\parallel > \sqrt{g_{\mathrm{s}}B}$ for the relevant case of gluons with $\sigma = +1$ and $l = 0$. This has a profound impact on the zero-point energy of the vacuum.

The sum over all (stable) modes of particles $(+)$ and antiparticles $(-)$ yields the vacuum energy, that is the expectation value of the Hamiltonian in the perturbative state $|B\rangle$ in the presence of the magnetic field $B$:

$$\langle B|\mathcal{H}|B\rangle = (-)^{2\sigma}\frac{1}{2}\left(\sum_+ E_+(B) - \sum_- E_-(B)\right) \equiv \mathcal{E}_0^\sigma(B)V. \qquad (3.8)$$

The coefficient of the zero-point energy density $\mathcal{E}_0^\sigma$ reflects the spin-statistics relation. The appearance of the lowest-angular-momentum states of the minimum allowable momentum leads for the gluon fields (after subtraction of the perturbative state and renormalization) to [35, 199, 200]

$$\mathcal{E}_0^{\mathrm{QCD}}(B) = \frac{b_0}{2}\frac{(g_{\mathrm{s}}B)^2}{4\pi}\log\left(\frac{(g_{\mathrm{s}}B)^2}{\Lambda^2}\right), \qquad (3.9)$$

where $b_0 = (1/2\pi)(11n_{\mathrm{c}}/3 - 2n_{\mathrm{f}}/3) > 0$ is as given by Eq. (14.14). Equation (3.9) proves that the vacuum state acquires an instability in the limit at $B = 0$, since the vacuum energy does not exhibit a minimum in this limit. We find a new minimum of the vacuum energy at a finite value of

$(g_sB)^2$. The scale of the 'condensation' field is determined by the renormalization scale $\Lambda$.

While these results prove the instability of the perturbative state $|P\rangle$, given the variational approach the ferromagnetic-vacuum model may be a very poor approximation to the actual vacuum structure of $|V\rangle$. Though the energy of the $|P\rangle$ vacuum is lowered, and we find a minimum at a finite value of the magnetic field $B$, it cannot be expected that we have, within this crude model, reached the lowest energy corresponding to the true state $|V\rangle$. Even so, Eq. (3.9) allows a first estimate of the latent energy involved in melting the (magnetic) QCD vacuum structure to be made:

$$\mathcal{B}_B \equiv -\mathcal{E}(B_{\min}) = \frac{b_0}{8\pi}(g_sB)^2_{\min} \lesssim \mathcal{B}. \tag{3.10}$$

$\mathcal{B}_B$ is seen as the variational approximation to the true value $\mathcal{B}$. The value at the minimum underestimates the true gain in energy within a more accurate vacuum structure model. To determine the scale of the magnetic field near the minimum of the energy density, we take as the average value of the square of the vacuum magnetic field the vacuum expectation value of the field operator squared, Eq. (3.3):

$$\frac{1}{2\pi^2}(g_sB)^2_{\min} \equiv \delta\frac{\alpha_s}{\pi}\langle V|F^a_{\mu\nu}F^{\mu\nu}_a|V\rangle. \tag{3.11}$$

$\delta$ is a positive number by definition. It can not be bigger than unity. The example of the quantum oscillator expression for $\langle x^2\rangle$ suggests that it is probably small relative to unity. The nonperturbative energy density of the vacuum state Eq. (3.10) is then of the magnitude

$$\mathcal{B} \gtrsim \frac{11 - \frac{2}{3}n_f}{8}\langle V|\epsilon\frac{\alpha_s}{\pi}F^2|V\rangle \simeq \delta\, 2.5 \text{ GeV fm}^{-3}. \tag{3.12}$$

We also note the Curie-point (the temperature at which the magnetic ferric structure melts) of the magnetic QCD state at temperature $T_{cr} \simeq \mathcal{B}_B^{1/4}$, at which one finds a strong first-order phase transition [192].

We infer from this exploration of a magnetic-vacuum model that the perturbative QCD vacuum $|P\rangle$ is unstable for $T < T_{cr}$, and that the transition to the true vacuum state involves a considerable release of latent heat. However, the quantitative results discussed here are merely providing an order-of-magnitude estimate. In fact, many other more complex semi-analytical models of the QCD vacuum structure were developed, of which the other most often addressed case is the instanton vacuum. In this approach, one draws on the (infinite) degeneracy of the unstructured state. A more thorough discussion of this model is offered in the monograph of Shuryak [245].

## 3.3 Chiral symmetry

The light u and d quark masses, which we have considered in table 1.1, are just slightly different when they are measured on the energy scale associated with the QCD vacuum structure, which is of the order of a few hundred MeV. This opens up an interesting interplay between the effective flavor symmetry of QCD and the vacuum properties. Recall that up and down quarks satisfy the relativistic Dirac quantum field dynamics, Eq. (13.79),

$$(i\gamma^\mu \partial_\mu - m)\Psi = 0, \tag{3.13}$$

from which there arise two identities,

$$\partial_\mu j_+^\mu \equiv \partial_\mu(\bar{u}\gamma^\mu d) = i(m_u - m_d)\bar{u}d, \tag{3.14}$$

$$\partial_\mu j_+^{5\mu} \equiv \partial_\mu(\bar{u}\gamma^\mu\gamma_5 d) = i(m_u + m_d)\bar{u}\gamma_5 d, \tag{3.15}$$

where $u$ and $d$ are the Dirac spinor-field operators representing the two light-quark flavor fields of current-quark masses $m_u$ and $m_d$, respectively. The subscript '+' reminds us that these currents 'lift' the 'down' quark to the 'up' quark; in the quantum-field-theory formulation this current is an iso-raising operator that increases the electrical charge by $+|e|$.

When the quark masses are equal, the isospin-quark current is conserved in Eq. (3.14), which implies that the Hamiltonian is symmetric under transformations that mix equal mass 'u' with 'd' quarks; this is an expression of the isospin-$SU(2)$ symmetry of strong interactions; this symmetry is broken by the electromagnetic and weak interactions, and by the difference in current-quark masses $m_u \neq m_d$, as seen in Eq. (3.14).

In case that the light quark masses were to vanish, by virtue of Eq. (3.15), the pseudo-vector isospin-quark current would also be conserved. Thus, when we are dealing with physical situations in which the current quark masses can be neglected, each isospin quark doublet operator $q \equiv (u, d)$ must be invariant under transformations that comprise two 'isospin rotations' associated with the two current-conservation laws.

When we are motivated by the physical properties of weak interactions, it is common to study the left- and right-handed quark fields

$$q_{L,R} \equiv \tfrac{1}{2}(1 \pm \gamma_5)q.$$

The reader is reminded that, for the right-handed case, the spin rotates right-handedly around the propagation axis, that is the spin and momentum vectors are pointing in the same direction; the 'helicity' is positive. It can be shown, on general grounds, that, for massless fermions, the helicity is conserved.

On forming the sum and difference of Eqs. (3.14) and (3.15), one finds that both the right- and the left-handed doublets form conserved iso-currents; thus the overall symmetry is $SU(2)_L \times SU(2)_R$. This is the

so-called chiral symmetry, i.e., 'handedness' symmetry. It is important to remember that this symmetry can be exact only if the masses of u and d quarks vanish exactly, and electro-weak interactions that distinguish the light quark flavor can be neglected. Since $m_{\mathrm{u}} + m_{\mathrm{d}} = 5\text{--}15\,\mathrm{MeV}$, we expect this nearly exact chiral symmetry to be manifesting itself strongly at the hadronic energy scale $\mathcal{O}(1)$ GeV, literally wherever we 'look'. Yet, there is no sign of the corresponding symmetry in the hadronic spectrum; there are no double doublets of hadronic parity states, e.g., we know that there is only one isospin doublet of nucleons (proton–neutron), not two: the second, chiral-symmetry-motivated opposite-parity, isospin doublet of nucleons is not observed. It would seem that chiral symmetry is badly broken by strong interactions, presumably the mass difference of quarks somehow matters.

However, the Adler–Weisberger sum rules, which relate weak and strong properties, confirm the presence of the intrinsic $SU(2) \times SU(2)$ symmetry in the elementary Hamiltonian. We refer to the recent discussion of Weinberg for a more comprehensive introduction to this rather important matter [268]. Nambu resolved this conflict between weak and strong interactions by proposing that the required symmetry-breaking mechanism is part of the *structure* of the strongly interacting vacuum state, and the physical hadron spectrum can indeed break the intrinsic (almost) chiral symmetry of the Hamiltonian [195]. Weinberg is of the opinion that the immediate acceptance of QCD as the dynamic theory of strong interactions was very much the result of a rather natural implementation in terms of practically massless 'current' u and d quarks (see Eqs. (3.14) and (3.15)) of these contradictory properties of weak and strong interactions.

The Nambu breaking of chiral symmetry in the hadronic spectrum requires that, in the limit that the quark masses vanish exactly, there would be an exactly massless Goldstone boson, a particle with quantum numbers of the broken symmetry, thus spin zero, negative parity, and isospin $I = 1$. Since the chiral symmetry of the strong-interaction Hamiltonian is not exact, the lowest-mass particle with these quantum numbers, the nearly massless pion state, expresses the properties of the massless Goldstone meson of strong interactions.

One could argue that the finite pion mass noticeable on the scale of hadronic interactions is removing from the hadronic spectrum most of the signature of chiral symmetry. The missing parity doublets of all strongly interacting particles are a 'direct product' of the Goldstone boson (pion) with all elementary hadron states. This, in turn, implies that many features of the hadronic spectrum, and possibly of the vacuum structure, should depend on the small, and seemingly irrelevant, current quark masses we see in Eqs. (3.14) and (3.15). How this could happen is not understood.

We show now that, in the limit of vanishing quark masses, we expect the pion mass also to vanish. This behavior plays an important role in the conceptual understanding of the vacuum structure of strong interactions. We consider matrix elements of the pseudo-scalar and the pseudo-vector quark currents between the vacuum state and one pion state,

$$\langle \pi^+(p)|\bar{u}(x)\gamma^\mu\gamma_5 d(x)|V\rangle \equiv -i\sqrt{2}p^\mu f_\pi e^{ip_\mu x^\mu}, \tag{3.16}$$

$$\langle \pi^+(p)|\bar{u}(x)\gamma_5 d(x)|V\rangle \equiv i\sqrt{2}g_\pi e^{ip_\mu x^\mu}, \tag{3.17}$$

where $p_\mu p^\mu = m_\pi^2 = (139.6 \text{ MeV})^2$. The form of the right-hand sides of Eqs. (3.16) and (3.17) arises by virtue of the Lorentz symmetry properties of the (true) vacuum state $|V\rangle$ and the $\pi^+$ state $|\pi^+(p)\rangle$. We consider the divergence $\partial_\mu$ of Eq. (3.16). Using relation Eq. (3.15), the following well-known result is found:

$$\boxed{m_\pi^2 f_\pi = (m_u + m_d)g_\pi.} \tag{3.18}$$

The matrix element $f_\pi$ is well known, since it governs the weak-interaction decay of pions, see, e.g., Weinberg, and the value $g_\pi$ is determined by sum rule methods [242, 243]:

$$f_\pi = 93.3 \text{ MeV}, \qquad g_\pi \simeq (350 \text{ MeV})^2. \tag{3.19}$$

Equation (3.18) implies that

$$m_u + m_d = 0.1 m_\pi, \tag{3.20}$$

a somewhat unexpected result in the present context, since the (current) quark masses are found to be much lighter even than that of the 'massless' pion.

Weinberg also presents an in-depth discussion of the exploration of the Nambu–Goldstone structure of the vacuum, in terms of symmetry relations between current-matrix elements (current algebra). In our context, the most important vacuum property involving quarks is the Gell-Mann–Oakes–Renner (GOR) relation, which, adapted to the quark language (see section 31 of [280], or [125]), implies a relation with the quark fluctuations (condensate) in the true vacuum:

$$\boxed{m_\pi^2 f_\pi^2 = 0.17 \times 10^{-3} \text{GeV}^4 \simeq -\tfrac{1}{2}(m_u + m_d)\langle \bar{u}u + \bar{d}d\rangle + \cdots.} \tag{3.21}$$

On dividing Eq. (3.21) by Eq. (3.18), we obtain

$$-f_\pi g_\pi = \tfrac{1}{2}\langle \bar{u}u + \bar{d}d\rangle|_{1\,\text{GeV}} \equiv \tfrac{1}{2}\langle \bar{q}q\rangle = -(225 \pm 9 \text{ MeV})^3, \tag{3.22}$$

where we have used the values of $f_\pi$ and $g_\pi$ given in Eq. (3.19). When Eq. (3.22) is combined with Eq. (3.21), and some of its generalizations, we can determine the values of current quark masses [105]. This shows how

the use of matrix-element properties and sum rules allows one to establish the physical values of the light quark masses presented in table 1.1.

We have introduced, in section 3.2, the condensates of glue, and above, of quark fields as if these were two quite independent physical effects of strong interactions. There remains an important question: is there a relation between glue-condensate melting (confinement-to-deconfinement transformation of the vacuum) and quark-condensate melting (the restoration of chiral symmetry)? One could be tempted to infer that the chiral symmetry-breaking features in QCD and gluon condensation have little in common. However, studies of restoration of symmetry of the vacuum at high temperature [103] have yielded contrary evidence: the two different vacuum structures of QCD always disappear together in the numerical studies as, e.g., the temperature is varied [103]. Model calculations [106, 107, 109, 251] employing mean-field configurations of gauge fields in the QCD vacuum suggest that it is the presence of the glue-field condensate which is the driving force causing the appearance of the quark condensate.

The mechanism connecting the two structures in the QCD vacuum (glue condensate, Eq. (3.3), and chiral condensate, Eq. (3.22)) is a major unsolved theoretical problem of strong-interaction physics. We will not pursue further in this book this interesting subject, which is undergoing rapid development.

## 3.4 Phases of strongly interacting matter

It is expected that, in nuclear collisions at relativistic energies, we attain conditions under which the structured confining vacuum is dissolved, forming a domain of thermally equilibrated hadronic matter comprising freely movable quarks and gluons. A qualitative sketch of the phase diagram of dense hadronic matter is shown in Fig. 3.1. The different phases populate different domains of temperature $T$ and baryon density $\rho_b$ presented in units of the normal nuclear density in heavy nuclei, $\rho_0 \simeq \frac{1}{6}$ nucleons fm$^{-3}$. For high temperatures and/or high baryon density, we have the deconfined phase. If deconfinement is reached in the nuclear-collision reactions, it 'freezes' back into the state containing confined hadrons during the temporal evolution of the small 'fireball', as indicated by the arrows in Fig. 3.1. Almost the entire $\rho$–$T$ region can be explored by varying the collision energy of the colliding nuclei.

The most difficult domain to reach experimentally is the one of low baryon number density, at high $T$, corresponding to the conditions pertaining in the early Universe. This demands extreme collision energies, which would permit the baryon number to escape from the central rapidity region, where only the collision energy is deposited; see chapter 5.
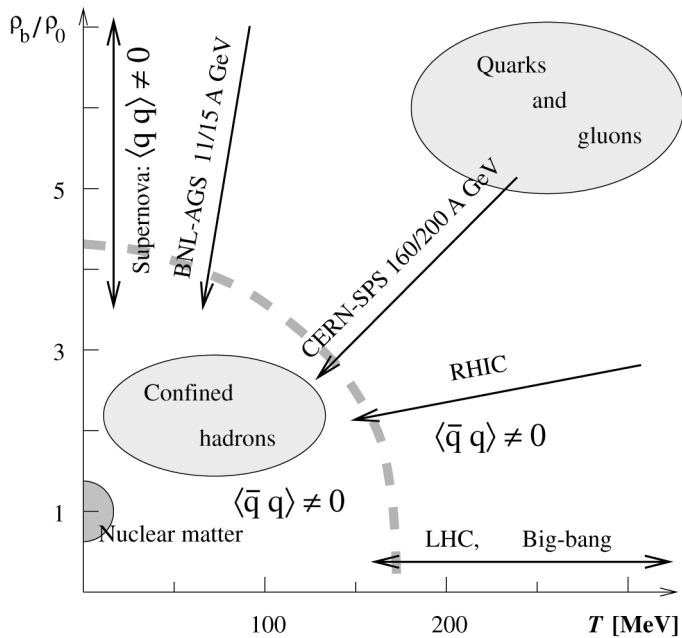
Fig. 3.1. The regions of the principal forms of hadronic matter are shown in the baryon-density–temperature plane. Their exploration with various accelerators is indicated, as are the domains relevant for cosmology and astrophysics. Also indicated is the behavior of the quark condensate.

The vertical arrow at the lowest temperatures, in Fig. 3.1, corresponds to the case of the stellar explosion of a supernova. Rather low-energy collisions at the AGS lead to such baryon-dense environments, which are more similar to nova explosions than they are to the early-Universe big-bang (horizontal arrow), which is better simulated by RHIC and future LHC experiments. In between these two extremes, we find the SPS conditions. The specific beam capabilities of the various accelerator facilities are complementary; section 5.1.

There are three regions indicated in Fig. 3.1 by the quark condensate, the expectation value of the quark fields $\langle \bar{q}q \rangle$, see Eq. (3.22), and $\langle qq \rangle$. The attractive quark–quark interaction present in some of the two-particle channels allows this di-quark color-condensate to form at low temperature and high quark density. We will not discuss the extensive work which recently addressed the properties of 'cold' quark matter, in which a 'color–flavor' locking (pairing) of quarks introduces yet other interesting structures in the deconfined state [31]. This color-superconductive phase had already been proposed early on in the study of properties of quark matter [53].

Recent studies have confirmed that the temperature at which such a color–flavor-locked phase of quark matter could exist is too low for an exploration in present-day laboratory experiments involving relativistic heavy-ion collisions [207]. At the temperature of interest in our studies, $T > 100$ MeV, the quark pairing will be largely dissolved. Work on this subject is rapidly evolving, for its current status we refer the reader to a recent review [227].

Where exactly an equilibrium transition between two phases occurs is determined from Gibbs' conditions for phase equilibrium. These establish the boundary between the physical phases considered, for bulk matter embedded in heat and particle-number 'baths'. These baths supply energy and particles to maintain given thermodynamic conditions. Although the circumstance of a nuclear-collision fireball is very different, the logic inherent in Gibbs' conditions will guide our understanding. The first condition is

$$P_1 = P_2, \tag{3.23}$$

which assures that there is no physical force acting on the phase boundary. We will momentarily return to discuss what happens when the phase boundary is in (relativistic) motion, see Eq. (3.28) below. The second Gibbs condition is

$$T_1 = T_2, \tag{3.24}$$

which assures that there is no radiative transport of energy between the phases.

How these conditions define the phase boundaries is illustrated in the $P$–$V$ diagram in Fig. 3.2. The pressure in two phases (QGP and HG) is considered at fixed temperature $T$ (and at given conserved baryon number $b$) as a function of volume $V$, at variable baryon density $\rho_{\rm b} = b/V$. We distinguish three domains in Fig. 3.2:

1. the HG region for $V > V_2$ (corresponding to $\rho_{\rm b} < \rho_2$), where the pressure rises modestly with the reduction of the volume;
2. the QGP region where the hadrons have disappeared at $V < V_1$ (corresponding to $\rho_{\rm b} > \rho_1$); and
3. the Van der Waals regime in the intermediate region from $V_1$ to $V_2$; a way to understand this domain is, e.g., that, at $V_1$, the progenitors of individual hadrons begin to emerge in the QGP phase in the form of a localized cluster of quarks. Similarly, beginning at $V_2$ and with decreasing volume, one can, e.g., consider clustering of individual hadrons into quark-drops [220].

Because clustering of hadrons leads naturally to the formation of drops of the QGP-like phase, we refer to the coexistence region, between $V_1$ and
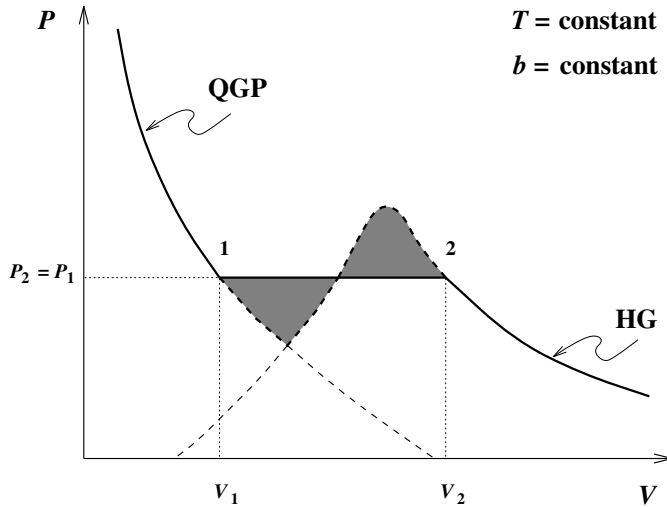
Fig. 3.2. The $p$–$V$ diagram for the QGP–HG system, at fixed temperature and baryon number; dashed lines indicate unstable domains of overheated and undercooled phases.

$V_2$, also as the mixed phase, comprising a mixture of hadrons and drops of QGP or perhaps hadron-like clusters of quarks and free quarks. To find out at which pressure the transformation between the phases occurs, at a given temperature $T$ (and fixed baryon number $b$), we find the value of the pressure, $P_1 = P_2 \equiv P_{12}$, connecting the volumes $V_1$ and $V_2$, requiring that the work done along the metastable branches vanishes:

$$\int_{V_1}^{V_2} (P - P_{12}) \, dV = 0. \tag{3.25}$$

The integrand is shown shaded in Fig. 3.2.

This Maxwell construction can be repeated for different values of $b$ and $T$, and the set of resulting points 1 and 2 forms then two phase-boundary lines shown on the left-hand side in Fig. 3.3, in the $(\rho_{\rm b}–T)$ plane. The Maxwell-construction line, seen in Fig. 3.2, is the vertical line connecting at fixed temperature $T$ the two different values of baryon density found – in general, a jump in baryon density (and energy density and entropy density) is encountered if a first-order phase transition occurs. The region of high $T$, at fixed $\rho_{\rm b}$, is associated with the deconfined QGP and the region of small $T$ with HG. The shape of the phase boundary is expressing the fact that a baryonless hadronic-gas phase cannot exist at a high enough temperature, and that dense compressed cold baryon matter will transform into the deconfined quark matter phase of quark matter.
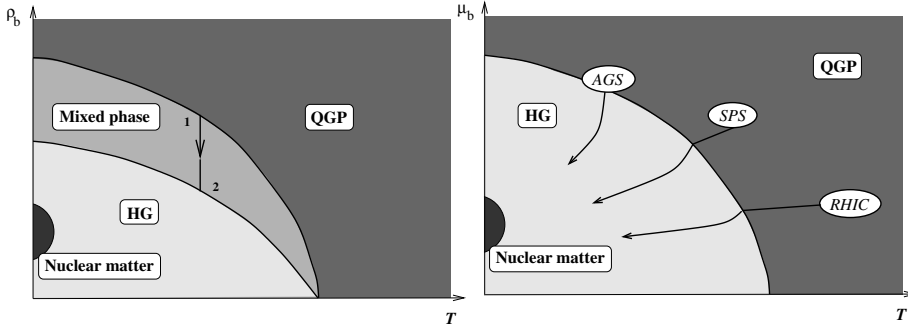
Fig. 3.3. Left: the regions of QGP and HG in the $(\rho_b\text{–}T)$ plane are separated by a band in which the phases coexist. The Maxwell-construction line corresponding to Fig. 3.2 is also shown, as is the path for the evolution of the Universe. Right: the same in the $(\mu_b\text{–}T)$ plane. The qualitative evolution of fireballs of dense matter created at the AGS, SPS, and RHIC is shown.

When we conserve the baryon number $b$ on 'average' and introduce the baryochemical potential $\mu_b$ as a variable, the representation of the phase boundary changes. According to the third Gibbs condition,

$$\boxed{\mu_1 = \mu_2,} \tag{3.26}$$

the two chemical potentials must have the same value at each given $T$ in order to assure that no transport of particles across the phase boundary occurs. Given Eq. (3.26), there is just a simple line separating any two hadronic phases in the $(\mu_b\text{–}T)$ plane, as is shown on the right-hand side in Fig. 3.3. There is a discontinuity of the energy density, baryon density, and entropy density across the phase boundary.

## 3.5 The expanding fireball and phase transformation

The lines shown on the right-hand side in Fig. 3.3 suggest the possible evolution of the fireball of dense matter formed in a heavy-ion collision. If a QGP fireball were indeed formed in the micro-bang, it will not expand along a fixed-temperature trajectory such as is encountered under the isothermal conditions of a heat bath. In our case, instead, entropy is the (nearly) conserved quantity for an isolated system subject to ideal flow. The evolution at constant entropy per baryon corresponds nearly to a straight line in the $\mu_b\text{–}T$ diagram in the domain of QGP (dark shaded), since the dimensionless ratio entropy per baryon is a function of other dimensionless variables – which, in the absence of significant scales other than $\mu_b$, and $T$ is $\mu_b/T$. A considerable change in temperature must occur during the evolution of a fireball, as is indicated in qualitative terms by the trajectories shown in the right-hand panel of Fig. 3.3.

A phase transition that is 'strong', i.e., involves significant changes in physical properties, will be easier to find. As a strong transition, we understand a case with, e.g., a jump in magnitude of the energy, or baryon density. Should such a strong phase transition separate the two phases, the super-cooling effect of a rapidly expanding (exploding) fireball of finite size could be much more pronounced.

We recall that both the QGP and the HG phases have metastable phase branches indicated by dashed lines in Fig. 3.2. However, now we look at these at constant entropy and variable temperature. Therefore, these domains are referred to as the undercooled plasma (continuation of 1 in Fig. 3.2), or the overheated hadronic-gas states (continuation of 2 in Fig. 3.2). Thus, the pressure of the QGP phase can evolve to be well below the transition pressure.

In fact, when a fireball of dense quark–gluon matter (phase 1) rapidly explodes, driven by the high internal temperature and pressure, it is possible that it continues even beyond $P = 0$. Namely, the fluid-flow motion of quarks and gluons expands the domain of deconfinement by exercising against the vacuum component in the total pressure a force originating from the collective velocity $\vec{v}_\mathrm{c}$.

Let $P$ and $\epsilon$ be the pressure and energy density of the deconfined phase in the local restframe, subject to flow velocity $\vec{v}_\mathrm{c} = (v_1, v_2, v_3)$. The pressure-tensor component in the energy–momentum tensor (compare with Eq. (6.6)) is

$$T^{ij} = P\delta_{ij} + (P + \epsilon)\frac{v_i v_j}{1 - \vec{v}^2}. \tag{3.27}$$

The rate-of-momentum-flow vector $\vec{\mathcal{P}}$ at the surface of the fireball is obtained from the energy-stress tensor $T_{kl}$:

$$\widehat{\mathcal{T}} \cdot \vec{n} = P\vec{n} + (P + \epsilon)\frac{\vec{v}_\mathrm{c}(\vec{v}_\mathrm{c} \cdot \vec{n})}{1 - \vec{v}_\mathrm{c}^2}. \tag{3.28}$$

The pressure and energy comprise particles (subscript p) and the vacuum properties:

$$P = P_\mathrm{p} - \mathcal{B}, \quad \epsilon = \epsilon_\mathrm{p} + \mathcal{B}. \tag{3.29}$$

Equation (3.28) for the condition $\widehat{\mathcal{T}} \cdot \vec{n} = 0$ reads

$$\mathcal{B}\vec{n} = P_\mathrm{p}\vec{n} + (P_\mathrm{p} + \epsilon_\mathrm{p})\frac{\vec{v}_\mathrm{c}(\vec{v}_\mathrm{c} \cdot \vec{n})}{1 - v_\mathrm{c}^2}, \tag{3.30}$$

and it describes the (equilibrium) condition under which the pressure of the expanding quark–gluon fluid is just balanced by the external vacuum pressure. On multiplying by $\vec{n}$, we find

$$\mathcal{B} = P_\mathrm{p} + (P_\mathrm{p} + \epsilon_\mathrm{p})\frac{\kappa v_\mathrm{c}^2}{1 - v_\mathrm{c}^2}, \tag{3.31}$$

where we introduced the geometric factor $\kappa$:

$$\kappa = \frac{(\vec{v}_\mathrm{c} \cdot \vec{n})^2}{v_\mathrm{c}^2}. \tag{3.32}$$

$\kappa$ characterizes the angular relation between the surface-normal vector and the direction of flow. Under the condition Eq. (3.31), the total QGP-phase pressure $P = P_\mathrm{p} - \mathcal{B}$, Eq. (3.29), is negative, as we set out to show.

Expansion beyond $P \to 0$ is in general not possible. A surface region of a fireball that reaches condition Eq. (3.31) and continues to flow outward must be torn apart. This is a collective instability and the ensuing disintegration of the fireball matter should be very rapid. We find that a rapidly evolving fireball that supercools into the domain of negative pressure is in general highly unstable, and we expect that a sudden transformation (hadronization) into confined matter can ensue under such a condition. It is important to note that the situation we have described could arise only since the vacuum-pressure term is not subject to flow and always keeps the same value.

## 3.6 QGP and confined hadronic-gas phases

We next seek to qualitatively understand the magnitude of the temperature at which the deconfined quark–gluon phase will freeze into hadrons. The order of magnitude of this transition temperature (if a phase change occurs) or transformation temperature (if no phase transition occurs, see Fig. 3.1) is obtained by evaluating where a benchmark value for the energy density occurs:

$$\epsilon_\mathrm{H} \simeq 3P_\mathrm{H} = 1 \text{ GeV fm}^{-3}.$$

The generalized Stefan–Boltzmann law (Eqs. (1.6) and (4.66)) describes the energy density $\epsilon$ and pressure $P$ as functions of the temperature $T$ of a massless relativistic gas:

$$P^\mathrm{SB} = \frac{1}{3}\epsilon^\mathrm{SB} = \frac{\pi^2}{90}gT^4. \tag{3.33}$$

The quantity $g$ is the number of different (relativistic) particle states available and is often called the 'number of degrees of freedom' or 'degeneracy'. In the deconfined phase,

$$g \equiv g_\mathrm{g} + \tfrac{7}{4}g_\mathrm{q}, \tag{3.34}$$

which comprises the contribution of massless gluons (bosons) and quarks (fermions). The relative factor $2 \times \frac{7}{8} = \frac{7}{4}$ expresses the presence of particles and antiparticles (factor 2) and the smaller fermion phase space, compared with the boson case, given the exclusion principle (factor $\frac{7}{8}$, section 10.5).

We use the degrees of freedom of quarks and gluons many times in this book. Here, we ignore the role of interactions. Gluons carry color and spin, and so do quarks, which, in addition, come in two ($n_f = 2$) flavors u and d; see table 1.1. Since at high temperatures the flavor count may include the strange quark, we leave $n_f$ as a variable. We obtain the following degeneracy in a QGP:

$$\text{gluons: } g_g = 2(\text{spin}) \times (N_c^2 - 1)(\text{color}) = 2 \times 8 = 16, \qquad (3.35a)$$
$$\text{quarks: } g_q = 2(\text{spin}) \times N_c(\text{color}) \times n_f(\text{flavor}) = 2 \times 3 \times n_f. \quad (3.35b)$$

When the semi-massive strange quarks are present, the effective number of 'light' flavors is $\simeq 2.5$. Thus, $g \simeq 40$ in Eq. (3.33), to be compared with just two directions of polarization for photons.

For a massless ideal quark–gluon gas, we find

$$T_H = 160 \text{ MeV}, \qquad \text{for} \qquad \epsilon_H = 1.1 \text{ GeV fm}^{-3}.$$

Hagedorn introduced this critical temperature in his study of the boiling point of hadronic matter [140]. Numerical simulations obtained by implementing QCD on a space–time lattice are available for zero baryon density, and these results confirm that, at approximately $T_H$, there is a phase transformation between confinement and deconfinement [160]. One also finds a rapid change in the behavior as the number of quarks and their masses $m_s$ and $m_q$ are varied.

The resulting complexity of the phase structure is shown, in Fig. 3.4, as a function of $m_s$ and $m_q$. In this qualitative representation, we look at the plane spanned by the light-quark mass $m_q = m_u = m_d$ and the strange-quark mass $m_s$. On two boundaries of Fig. 3.4 these masses are infinite. Only near the origin is the effective number of massless flavors three, along the diagonal we have three massive flavors. Depending on the actual values of quark masses, different phase properties emerge [162].

The theoretical finding that a smooth crossover between the confined and deconfined phases is a possibility raises the question of how to understand qualitatively the gradual onset of color (quark, gluon) mobility. A gradual change implies that free quarks can coexist with confined hadrons. This then also suggests that liberation of quarks is possible since permanent confinement could be assured only at zero temperature, a mathematical limit. For any finite excitation of the system, quark mobility remains, akin to the transition of an atomic gas to an electron–ion
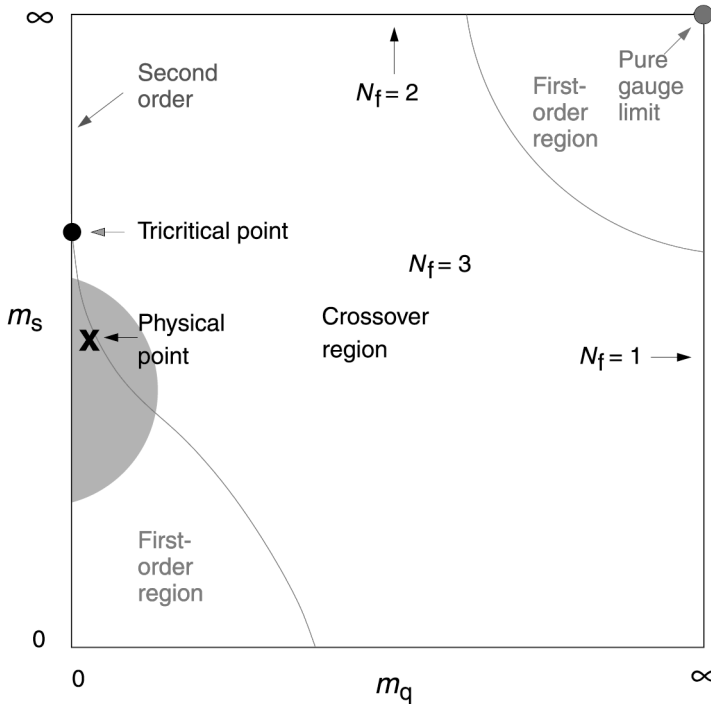
Fig. 3.4.   The nature of finite-temperature QCD phase structure as a function of quark masses $m_q$ and $m_s$.

plasma. However, experimental searches for quarks have not succeeded [186]. The experimental limits which were set suggest that confinement is a fundamental physical property. This being the case, we are of the opinion that, in the physical world, the transformation from the confined to the deconfined phase is a discontinuous phase transition, most likely of first order. For this reason, we placed the physical quark-mass point within the region of first-order phase transition in Fig. 3.4. This topical area is undergoing a rapid evolution.

# 4 Statistical properties of hadronic matter

## 4.1 Equidistribution of energy

The physical tools required to describe in further detail the properties of hot hadronic matter are much like the usual ones of statistical physics, which we briefly introduce and review. A more detailed analysis will follow.

Consider a large number $N$ of identical coupled systems, distinguishable, e.g., by their energies $E_i$. To simplify the matter, we assume that